Roman and modern slag at S. Domingos mine (IPB, Portugal): compositional features and implications for their long-term stability and potential reuse

A. Mateus*

Faculdade de Ciências,
Departamento de Geologia and CeGUL,
Universidade de Lisboa,
Ed. C6, Piso 4, Campo Grande,
1749-016 Lisboa, Portugal
Fax: +351351-217500064
E-mail: amateus@fc.ul.pt
*Corresponding author

A. Pinto

CREMINER,
Faculdade de Ciências,
Universidade de Lisboa,
Ed. C6, Piso 4, Campo Grande,
1749-016 Lisboa, Portugal
E-mail: ampinto@fc.ul.pt

L.C. Alves

Departamento de Física,
Instituto Tecnológico e Nuclear,
Estrada Nacional nº10, 2686-953 Sacavém, Portugal
E-mail: lcalves@itn.pt

J.X. Matos

Laboratório Nacional de Geologia e Energia,
U.I. Recursos Minerais e Geofísica,
R. Frei Amador Arrais 39 r/c Ap. 104,
7801-902 Beja, Portugal
E-mail: joao.matos@lneg.pt

J. Figueiras

Faculdade de Ciências,
Departamento de Geologia and CREMINER,
Universidade de Lisboa,
Ed. C6, Piso 4, Campo Grande,
1749-016 Lisboa, Portugal
E-mail: jmvf@fc.ul.pt

N.R. Neng

Faculdade de Ciências,
Departamento de Química e Bioquímica,
Universidade de Lisboa,
Ed. C8, Piso 2, Campo Grande,
1749-016 Lisboa, Portugal
E-mail: ndneng@fc.ul.pt

Abstract: S. Domingos ores have been exploited for Cu and S from antiquity to 1966. Slag is composed of Fe-, Ca-, Zn- and Pb-rich silicate glass, fayalite, hedenbergite, Fe-spinel, and blebs of Fe-, Cu-, Zn- (and Pb-)sulphides, minor sulphosalts and Cu-Zn-Pb-*iss* with evidence for low-T exsolution and reactions. Silicates and oxides often crystallised far from equilibrium out of undercooled melts. Weathering leads to Fe-(hydro)oxide + digenite ± Fe-, Cu- and Pb-sulphate, Ca, Zn and Pb loss from glass and acid drainage. The slag is an excellent aggregate raw material but its chemical instability calls for preliminary processing, which might lead to economic metal recovery.

Keywords: metal-rich slag; long-term slag stability; slag reuse potential; ore-processing wastes.

Reference to this paper should be made as follows: Mateus, A., Pinto, A., Alves, L.C., Matos, J.X., Figueiras, J. and Neng, N.R. (2011) 'Roman and modern slag at S. Domingos mine (IPB, Portugal): compositional features and implications for their long-term stability and potential reuse', *Int. J. Environment and Waste Management*, Vol. 8, Nos. 1/2, pp.133–159.

Biographical notes: António Mateus earned his Geology and PhD (Geology – Metallogeny) from the University of Lisbon in 1985 and 1995, respectively. Currently, he is professor of the Faculty of Sciences of the University of Lisbon. His research interests cover different topics, mostly in interface fields between mineralogy, geochemistry, ore-forming processes, rock deformation and fractals in geosciences, and has authored or co-authored 15 technical reports and 124 scientific articles published in specialised journals, books and conferences proceedings. He is a member of SGA, MSA, SGP and APG.

Álvaro Pinto earned his MSc in 1999 from the University of Lisbon (UL). He has served as an ore-mineralogist at the Neves Corvo mining company (Somincor) and as Teaching Assistant at the Department of Geology of the UL. Presently, he is a mineralogist at the National Museum of Natural History – UL. At CREMINER – FCUL, he is in charge of consulting

services and links with industry on applied mineralogy studies for exploration, exploitation, mineral beneficiation and environmental impacts in mining industry. His research work as a PhD student is centred on ore mineralogy, metallogeny and ore mineral geochemistry, and he has published several articles particularly concerning the Neves Corvo ore-deposit metallogeny.

Luís Cerqueira Alves obtained his MSc (1993) and PhD (2004) in Physics from the Lisbon University and has authored or co-authored more than 60 scientific articles in international journals. He is a researcher at Instituto Tecnológico e Nuclear (ITN) and has been working in the development and application of ion beam analytical techniques with the 2.5MV Van de Graaff accelerator installed at ITN, in particular using a Nuclear Microprobe. The main applications of the implemented techniques have been performed in material science (mainly the study of advanced materials intended to be used in Nuclear Fusion Reactors), environmental (chiefly source emission monitoring and identification of air particulate matter, besides the study of lichens as pollution biomonitors) and mineralogy fields.

João Xavier Matos earned his BSc in Geology from Lisbon University in 1986 and his MSc in Economic Geology from the same University in 1992. Presently, he is Assessor Geologist of the Mineral Resources and Geophysics Research Unit of the Portuguese Geological Survey (LNEG). Since 1990, he worked in the field of mineral deposits exploration, metallogeny and geological mapping of abandoned mines (including mining waste distribution, mine safety and geotechnical mapping). His responsibilities included the collaboration with 28 RD national and international projects related to mining risk, geochemistry, geophysics, regional geology and mining heritage. He has authored or co-authored over 110 scientific articles, 35 technical reports and 17 conferences.

Jorge Figueiras earned his PhD in 1997 from the University of Lisbon, where he is now an Assistant Professor. His research work centres on environmental geochemistry, and he has authored over 50 scientific articles published in specialised journals and conferences proceedings. He also works on metal geochemistry dispersed around ancient mining centres.

Nuno da Rosa Neng received his BSc in Chemistry from the University of Lisbon in 2005and he is currently finishing the MSc in Biomedical Inorganic Chemistry at the same University. He researches in analytical chemistry, particularly on the development and application of methods involving chromatographic (GC and LC), electrophoretic (CE), hyphenated techniques (GC-MS and LC-MS), atomic absorption spectrometry and X-ray powder diffraction techniques. Special attention is being given to modern approaches on sample preparation of complex matrices, namely Solid Phase Extraction (SPE), Solid Phase Micro-Extraction (SPME) and Stir Bar Sorptive Extraction (SBSE).

1 Introduction

Worldwide and incessantly, the ore-processing industry produced and still generates a huge amount of wastes and residues that demand a careful sorting and management, thus

contributing to the goals implicit in the paradigm of raw-materials sustainability (e.g., Evanko and Dzombak, 1997; Moore and Luoma, 1990; Ally et al., 2001). This can be achieved by means of different strategies in accordance with the ore nature and the procedures used on its exploitation or employed in metal extraction, always with due attention paid to the changes potentially experienced by old/abandoned piles of mining wastes and residues laid down for long time spans (e.g. Kucha et al., 1996; Gee et al., 1997; Ally et al., 2001). However, irrespectively of the strategy designed, a proper characterisation of the present and past wastes and residues is unavoidable, including necessarily a comprehensive analysis of their compositional features and geochemical stability. As a result of such analysis, it would be possible to

i separate the true wastes from residues

ii indicate the best procedure to operate the waste dumping and, if necessary, the subsequent site monitoring

iii address conveniently hazardous waste problems (acid drainage, metal dispersion, etc.)

iv search for new ways of residue reuse

v promote a more powerful reprocessing technology to recover additional by-products from existing residues.

Slag is a common and voluminous industrial residue that cannot be avoided even after improvement (process reengineering) of smelting, foundry, and other metallurgical and combustion processes. The physical–chemical characteristics of slag make it suitable for reuse in a wide range of applications (Atzeni et al., 1996; Eusden et al., 1999) and, in some circumstances, for recycling to extract some of its components via reprocessing (Nagasua, 1979; Tümen and Bailey, 1990; Ziyadanoğullari and Ziyadanoğullari, 1999; Ally et al., 2001). This reprocessing is especially relevant for some types of metal-rich slag, although a study of each individual case is needed because of variable technical, environmental and economic factors. Nonetheless, any assessment on slag recovery potential depends, primarily, on a deep knowledge of their component phases (granularity, composition and relative abundance). And even in the presence of strong constraints hindering the reclamation of valuable metals from the slag, such knowledge remains crucial to decisions on how to dump the slag according to environmentally sound management practices.

Several studies focusing on metal-rich slag have been published recently (e.g., Chaudhuri and Newesely, 1993; Kucha et al., 1996; Gee et al., 1997; Ettler et al., 2001), but most of them provide only limited information about the compositional features of its major phases. In this work, the slag piles of the abandoned S. Domingos mine (IPB, Portugal) are examined. These piles display distinct features and represent some of the industrial residues produced during the mining activity in Roman and modern (1934–1962) times. The data reported here are discussed with a threefold objective:

i to identify the metals present and their distribution in the slag-forming phases

ii to assess slag stability when weathered over a long period of time

iii to evaluate the slag reuse potential.

2 The S. Domingos mine

S. Domingos is a volcanogenic massive sulphide deposit located in the Portuguese segment of the IPB (Figure 1(**A**)) that was subjected to intermittent but significant exploitation from Roman times to 1966 (Webb, 1958; Vara, 1963; Carvalho, 1971; Oliveira and Silva, 1990; Silva et al., 1997; Barriga et al., 1997; Gaspar, 1998; Carvalho et al., 1999; Matos et al., 2006a). The ore-body consists of a sub-vertical lens containing ≈25 Mt of sulphides (mostly pyrite), which is located on top of a Volcanic-Sedimentary Complex (VSC) sequence comprising black shales and different meta-volcanic rocks dated from Late Famennian to Late Visean (Figures 1(**B**) and 2(**A**)). This suite is preserved in a sigmoid-shaped tectonic-sheet developed during the Variscan Orogeny, contacting meta-sediments belonging to the Phyllite-Quartzite (Late Strunian) and Represa (Late Famennian) Formations (Matos, 2004; Matos et al., 2006a). The outcropping portion of the ore-body is intensely weathered (Figure 2(**B**)), forming a thick iron-hat that was actively exploited in Roman times, as documented by artefacts, access-galleries and remnants of slag piles and totally exploited during the 19th century. Modern exploitation was carried out by the Mason & Barry Company between 1857 and 1966, using an open pit that reached 120 m depth and underground works reaching a depth of 420 m (Figure 2(**B**)); at the 150 m level, there were mining works from the main water pump shaft (Malacate nº 6) to the air pump shaft (nº 7) located ca. 1080 m away in the eastern sector of the mine (Mason & Barry Company, 1962; Matos et al., 2006b), see Figure 2(**A**).

As a result of this long mining activity, large volumes of wastes/residues were produced and dumped at several locations (Table 1). 14.7 M m^3 of mining waste of several types are estimated to be present at S. Domingos, accumulated to thicknesses varying very irregularly from 14 m near the open pit to less than 1 m at the locations furthest downstream (Matos, 2004; Matos and Martins, 2006). Comprehensive mapping of these discarded products (Figure 3) enabled the separation of different types of piles whose composition and internal organisation reflect the successive methods used in the exploitation work and in ore treatment/benefiting. All these piles contain significant amounts of metals (e.g., Batista, 2000; Matos et al., 2003; Bryan et al., 2006) that reflect primarily the efficiency of the methods used in ore exploitation and processing. The slag piles are just a small part (≈8%) of the total mine residues accumulated at S. Domingos; yet as either a source of pollution (of soils, surface and groundwaters), or a potentially valuable by-product, they deserve special attention.

Figure 1 (**A**) Geographical position (inset) and schematic geological map of the Iberian Pyrite Belt showing the location of the main mining centres (adapted from Oliveira et al. (2006)) and (**B**) Simplified geological map of the São Domingos mining area (Hayford-Gauss coordinates in km); adapted from Matos (2004) and Oliveira and Matos (2004): *Geology*: 1. Quaternary alluvium sediments; 2.-5. Palaeozoic Basement (South Portuguese Zone): 2. Mértola Fm. (Upper Viséan); 3. Volcano Sedimentary Complex (Late Famennian – Late Viséan); 4. Undifferentiated Phyllite-Quartzite Group (Frasnian - Late Famennian), Represa Fm. (Late Famennian) and Barranco do Homem Fm. (Famennian?); 5. Gafo Fm. (Lower Frasnian); 6. Thrust; 7. Fault; 8. Geological limit. *Mining*: 9. Mining wastes and landfills; 10. Mine infrastructures; 11. Acid water dam/lagoon; 12. Clean water dam; 13. Abandoned mine railway; 14. Mine channel; 15. Stream

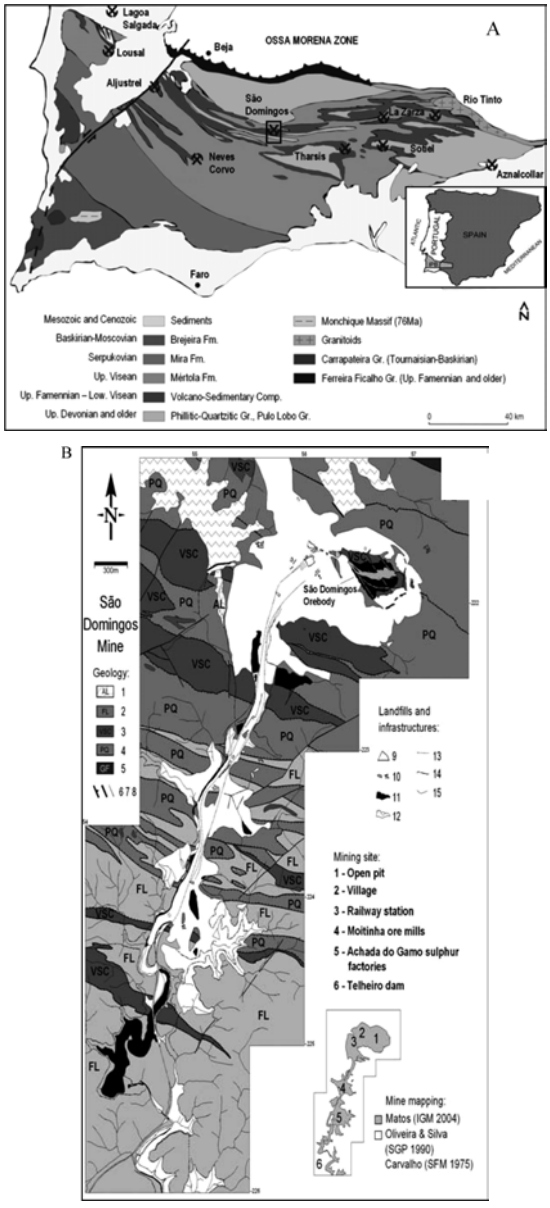

Figure 2 (**A**) Geological map and main tectonic framework (inset) of the S. Domingos open pit (Hayford-Gauss coordinates in km); adapted from Matos et al. (2006). 1.-7. Late Famennian – Late Visean Volcano Sedimentary Complex: 1. Metadolerito; 2. S. Domingos orebody projected to the water surface in the flooded open pit; 3. coarse polymict felsic volcaniclastic metabreccia; 4. Porphyritic metarhyolites/metarhyodacites 5. Basic meta-volcanics; 6. intermediate meta-volcanics; 7. footwall black shales; 8. Late Strunian Phyllite-Quartzite Group (shales and quartzites); 9. Late Fammenian Represa Fm. (black shales with disseminated pyrite and banded siltitic shales); 10. Fammenian (?) Barranco do Homem Fm. (phyllites, greywackes, quartzwackes); 11. stockwork; 12. hydrothermal chloritic alteration: 13. hydrothermal silicic alteration; 14. Cu minerals in tectonic cleavage and fractures; 15. acid water spring; 16. thrust; 17. fault; 18. geological boundary; 19. strike and dip of strata; 20. strike and dip of the main tectonic cleavage; 21. Intersection lineation of stratification and tectonic cleavage; 22. Diaclase dip and strike D_1; 23. Tectonic movement along faults (inset only); 24. landfill and tailings; 25. shaft; 26. modern gallery; 27. roman gallery; 28. flooded open pit, acid water level 107 m amsl; 29. mining heritage pedestrian track. The numbered light lines are topographic contours (elevation in meters) and (**B**) N-S cross section through the S. Domingos orebody. Legend as in (**A**)

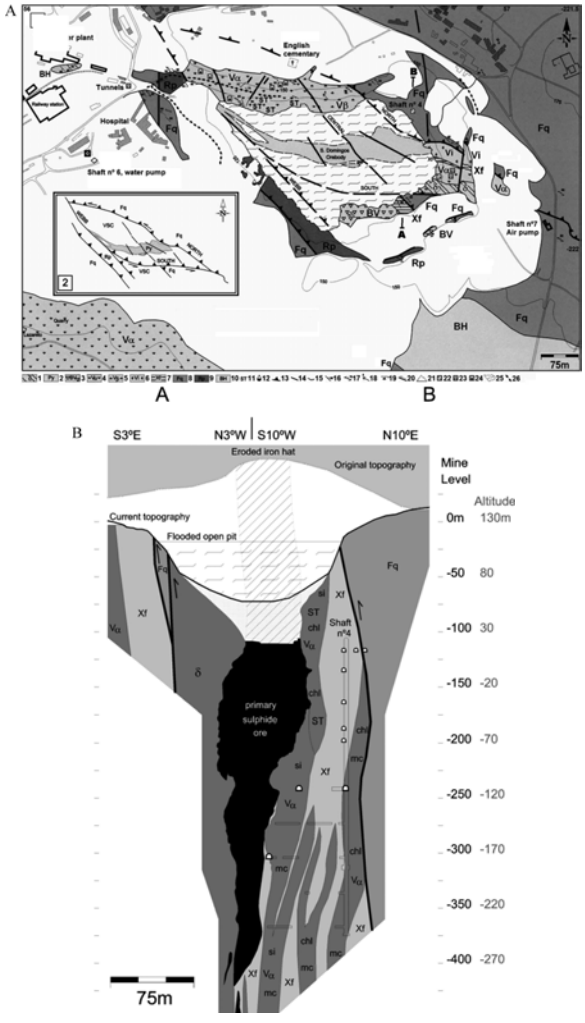

Figure 3 Spatial distribution of the mining waste and residue piles in the S. Domingos mining area (Hayford-Gauss coordinates in km); adapted from Matos (2004). The ore treatment procedures outlined in the diagram were in place during the last decennia of mining operations. *Geology*: 1. Alluvium; 2. Palaeozoic basement. *Mining waste*: E1. Modern slag; E2. Roman slag; E3. Iron-hat material; E4. Meta-volcanic rocks and shales; E5. Shales; E6. Finely crushed sulphide ore; E7. Roasted sulphide ore. *Landfills and infrastructures*: F. Water-laid contaminated materials in seasonally flooded areas; L. Mine/urban contaminated landfills; AMD. Soilless areas due to ancient protracted acid mine water flow; LF. Sulphide ore leaching plateau; 3. Acid water dam/lagoon; 4. Clean water dam; 5. Cu cementation tank; 6. Orkla sulphur factories; 7. Railway station; 8. Power plant; 9. Abandoned mine railway; 10. Mine canal; 11. Stream

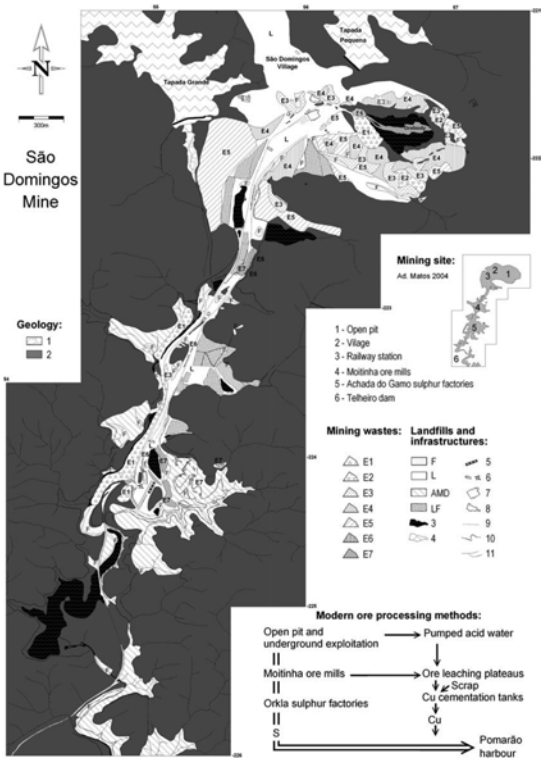

3 Roman and modern slag piles

The Roman Slag (**RS**) piles are preserved in two places adjoining the modern open pit and cover an area of *ca.* 28173 m^2 (Table 1; Figure 4); the NE pile is thicker (up to 2 m currently remaining), rests on a palaeo-soil and has a very poor centimetric soil layer developed on it. The eastern pile is covered by 19th century mine waste. According to archaeological evidence quoted in Custódio (1996), the Roman mining activity seems to have occurred in the upper 50 m of the iron-hat, probably in its Cu-rich domains, which no longer exist. Therefore, taking as reference the composition of the present unexploited

iron-hat may lead to erroneous evaluations of the ore-processing efficiency at that time. Concurrently, the lack of reliable data on the details of the Roman smelting technologies in oxide-ore processing creates additional difficulties in slag data interpretation.

Table 1 Areas occupied by different classes of mining wastes and residues at the S. Domingos mining centre

	Waste/residue	*Roman period*	*XIX century*	*1930–1966*	*Main location*
Slag	Roman	28173 m^2 (a)			Open-pit
	Modern			109717 m^2	Open-pit, Moitinha, Achada
Fe-oxides from roasting			3606 m^2		
Sulphide ore	Ashes			27968 m^2	Moitinha, Achada
	Fragmented			4007 m^2	Open-pit
	Blocks			4028 m^2	Moitinha, Achada
Iron-hat	Fragmented		22071 m^2		Open pit, Village
	Coarse blocks (b)		82838 m^2		Open pit, Village
Host rocks	Meta-volcanic fragments (strongly weathered and enriched in Fe-(hydr)oxides	?	104923 m^2		Moitinha, Achada
	Meta-volcanic and shale fragments		81697 m^2		Open-pit
	Shale fragments		252517 m^2		Open-pit
Acid waters	Lagoons/dams (accumulated)	?	273250 m^2		Open-pit, Moitinha, Achada, S. Domingos Valley
	Total soil destruction (c)	?	1186591 m^2		Moitinha, Achada, S. Domingos Valley
Cementation tanks				1088 m^2	Achada
Leaching tanks			152306 m^2	?	Moitinha
Clays (leaching process)				120288 m^2	S. Domingos Valley
Industrial landfills			501265 m^2		S. Domingos Valley
Area affected by mining activity		>255300 m^2 (d)	2963900 m^2 (e)		From open-pit into S. Domingos Valley

(a) Estimated original area of 255300m^2; (b) Area outside the village only; (c) due to artificial diffuse surface circulation aimed at evaporating acid water; (d) Inferred; (e) 3076900m^2 if 113000m^2 of contaminated urban landfill (village houses built over the old tailings (19th century) comprising fragments of iron-hat and altered meta-volcanic rocks) are included. Surface data obtained with CAD analysis over the geological and mining mapping (Matos, 2004).

The modern slag piles represent ≈7.4% of the total residue accumulation and can be found in two distinct sites:

1 on the southern wall of the open pit

2 near the Achada do Gamo sulphur factory/Moitinha ore-mills; together, these piles cover an area of *ca.* 109717 m^2 (Table 1; Figures 4 and 5), with a wide range of thicknesses.

As stated in the Technical Reports of the Mason & Barry Company, this slag is an output of the Orkla metallurgic process designed to obtain sulphur from low-grade base metal sulphide ores (Cu < 1.5%, Zn < 3%, Pb < 2% and 45–48% S), mainly consisting of pyrite with accessory amounts of chalcopyrite, sphalerite and galena and traces of other sulphides and sulphosalts (e.g., Vara, 1963). The first (and main) furnace dedicated to sulphur production was installed in 1934 and showed a recovery efficiency of ca. 55%. The second furnace, built in 1944 and originally intended to concentrate only Cu matte, never fulfilled the desired goals and was readjusted in 1946 for sulphur production; it was definitely closed in 1962, showing at that time recovery efficiencies below 51%. It should be noted that the present distribution of the slag piles results from a major operation dating from the 1950s, which consisted in the removal of large amounts of the earlier slag produced in the main furnace from its initial location to the S wall of the open pit. The reasons for this relocation are not stated in the old reports, but it is probable that the relocated slag was dumped against the open pit wall to stabilise it in a zone where geotechnical instability is well known to occur (Matos et al., 2006b).

Figure 4 Detail of Figure 3, showing the area around the open pit (Hayford-Gauss coordinates in km); adapted from Matos (2004). 1. Volcano-Sedimentary Complex; 2. Sulphide ore; 3. Undifferentiated Phyllite-Quartzite Group, Represa and Barranco do Homem Fms. 4. Thrust; 5. Fault; E1. Modern slag; E2. Roman slag; E3. Iron-hat materials; E4. Meta-volcanic rocks and shale piles; E5. Shale piles; E6. Finely crushed sulphide ore; L. Mine/urban contaminated landfills; F. Water laid materials in seasonally flooded areas; 6. Acid water spring; 7. Mine shaft; 8. Modern gallery; 9. Roman gallery; 10. Abandoned mine railway; 11. Open pit flooded with acid water to 105 m above mean sea level; 12. Mining heritage pedestrian track. The sulphide ore-body shown is a projection of its location and limits to the water surface in the flooded open pit

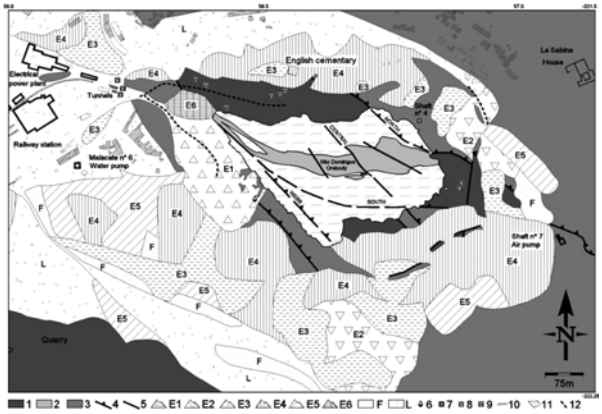

Figure 5 Details of Figure 3, showing the areas of Moitinha and Achada do Gamo industrial facilities; adapted from Matos (2004). E1. Modern slag; E3. Gossan; E6. Finely crushed sulphide ore; E7. Roasted sulphide ore; F. Leached materials in seasonal flooded areas; L. Contaminated landfills; AMD. Soilless areas due to ancient protracted acid mine water flow; 1. Acid water lagoon; 2. Cu cementation tank; 3. Orkla sulphur factories; 4. Abandoned mine railway; 5. Mine channel; 6. Stream

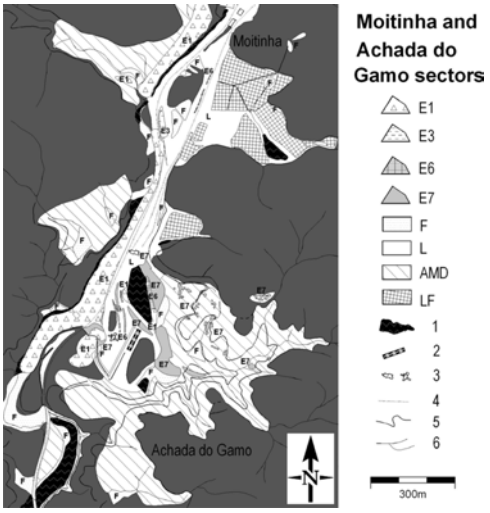

3.1 Sampling and analytical methods

A sampling programme was carried out in the NE pile of **RS** and in the modern slag piles adjoining the abandoned open pit and the old smelter facility at Achada do Gamo (Figures 4 and 5). The collected samples were comprehensively examined by means of optical microscopy, X-ray diffraction (XRD), scanning electron microscopy with energy-dispersive X-ray spectroscopy (SEM-EDS), Electron Probe Microanalysis (EPMA) and particle-induced X-ray emission microanalysis (μPIXE). Multi-element chemical analyses were performed at the Activation Laboratories Ltd. (Canada) after fine grinding of representative samples of each slag in a tungsten carbide mill; solutions for ICP/MS and INAA determinations were obtained by acid total digestion. Additional quantitative data were obtained by image analysis techniques, using the Leica QWin V3 software coupled to an optical microscopy digital image acquisition system.

Fine powders of selected slag samples, spread on silicon plates (Philips PW 1817/32), were used to obtain XRD patterns with a Philips PW 1710 powder diffractometer using CuKα radiation, a curved graphite crystal monochromator and a PW1820 Bragg-Brentano goniometer; subsequent phase identification was based on the Mineral Powder Diffraction File Databook (Bayliss et al., 1993).

SEM-EDS data were acquired with a JEOL JSM-6301F scanning electron microscope coupled to an OXFORD INCA/ENERGY 350 microanalyses system; the equipment was operated using an accelerating voltage of 15 kV and full-scale scanning.

EPMA data were obtained with a five-channel wavelength-dispersion JEOL-JXA-8500F. Opaque and non-opaque minerals were analysed under different instrumental conditions. For non-opaque minerals, an accelerating voltage of 20 kV and a beam current of 15 nA were used; the corresponding values for opaque minerals are 20 kV

and 20 nA. Minerals and pure metals were used as standards and the beam diameter was set to 1 μm.

For μPIXE, an Oxford Microbeams nuclear-microprobe-type set-up (Alves et al., 2000) was used to focus a 2 MeV proton beam generated with a Van de Graaff accelerator. X-ray spectra were accumulated with an 80 mm^2 Si(Li) detector (resolution: 155 eV) located at a backward angle of 45º and at a distance of 25 mm from the sample. The spatial resolution of the beam was initially set to 3 μm, with a beam current close to 200 pA. The focused beam was raster-scanned over some previously defined regions of interest of the samples, and two-dimensional X-ray elemental maps were obtained. From those maps, some spots were chosen to perform μPIXE point analysis. Trace amounts of Ag, Cd, In, Sn and Sb were determined in some selected spots using a mixed filter of 50 μm Mylar, 330 μm Al and 1 mm Perspex in front of the Si(Li) detector, with a beam current of 5 nA. Mapping, data acquisition and data manipulation were done with the OM-DAQ programme (Grime and Dawson, 1995), whereas spectra fitting and semi-quantitative results were obtained with the GUPIX computer package (Maxwell et al., 1995), which accounts for matrix and secondary fluorescence corrections.

3.2 Macroscopic features

The **RS** is composed of irregular but massive centimetric black-brownish fragments, invariably covered by a discrete reddish coating; these fragments are strongly packed together, preserving an incipient interstitial matrix of fine-grained slag. The modern slag piles show distinct macroscopic features:

1 the pile dumped against the SW wall of the abandoned open pit (**S1**) comprises fine (and oxidised) fragments of granular slag and coarse fragments of massive black-greyish slag that display discontinuous weathering coatings (either consisting of Fe-hydroxides or of Cu and Fe sulphates)

2 the piles near the old smelter at Achada do Gamo (**S2**) are more homogeneous in granularity and include coarse-grained, massive black slag fragments with glassy appearance that rarely display macroscopic evidence of significant weathering effects; sometimes, vitreous material of grey-greenish colour also occurs.

According to the available technical data, molten slag was discarded and simply allowed to cool in the atmosphere, solidifying under environmental conditions. As mentioned earlier, a significant part of the **S1** pile records a relatively late operation of slag disposal and management, leading to heterogeneous mixing of air-cooled slag (the most abundant) and granular slag. The latter, more porous and apparently more reactive, prevails in the northern domain of the **S1** pile and is a result of sporadic rapid water and air quenching; this slag displays typically a lower specific gravity and is composed of angular fragments that show variable degrees of oxidation.

3.3 Slag chemical composition

Results of the multi-element chemical analyses performed in representative slag samples are presented in Table 2.

Chemically, all slag types are very similar in what concerns their major and lithophile elements composition. The slag is dominated by Fe and Si, with Fe concentrations

up to 41 wt% in the modern slag and 37 wt% in the **RS**. Ca is always rather low, from a maximum of 6.3 wt% CaO in the **S2** slag and a minimum as low as 1.2 wt% CaO in **RS**. This reflects the scarcity of Ca in the ores of S. Domingos and also the fact that neither the Romans nor the Barry and Mason Company have significantly used Ca-bearing additives in their metallurgical procedures. All other lithophile major element oxides (except Al) are below 1 wt%, as should be expected from the general composition of the ores; note also that the slag is very poor in volatile elements.

Table 2 Average chemical composition of the three slag types found at S. Domingos (selected elements only). < and > indicate below detection limit and above saturation threshold of the method, respectively. – not analysed

		S1	*S2*	*RS*
SiO_2	wt%	28.48	34.44	37.70
Al_2O_3	wt%	1.51	1.97	3.93
Fe_2O_3	wt%	58.15	58.52	52.86
MnO	wt%	0.05	0.05	0.07
MgO	wt%	0.70	0.46	0.40
CaO	wt%	4.95	6.28	1.14
Na_2O	wt%	0.02	0.15	0.25
K_2O	wt%	0.22	0.26	1.04
TiO_2	wt%	0.107	0.373	0.688
P_2O_5	wt%	0.05	0.04	0.20
LOI	wt%	3.49	<0.01	<0.01
S	wt%	5.64	2.04	0.822
Au	ppb	115	123	2190
Ag	ppm	8.6	4.3	74.5
As	ppm	180	112	1730
Ba	ppm	62	133	1240
Bi	ppm	47	<2	28
Cd	ppm	2.7	4.0	–
Co	ppm	178	261	14
Cu	ppm	2930	3280	252
Mo	ppm	6	17	67
Ni	ppm	17	20	8
Pb	ppm	3820	>5000	>5000
Sb	ppm	108	492	2310
Se	ppm	<3	<3	95
Sr	ppm	46	55	124
V	ppm	34	33	108
Zn	ppm	9130	>10000	83

The S content of the slag varies from type to type, decreasing from 5.6 wt% in **S1** to 2.0 wt% in **S2** to 0.8 wt% in **RS**. The lower S contents of **RS** is primarily due to the fact that the Romans were exploiting the S-poor iron-hat whereas the modern slag was produced from the primary sulphide ore; technological differences between the Roman and the

modern epochs and also, perhaps, different metallurgical aims (Cu vs. S extraction) cannot be entirely ruled out as accessory causes of the contrasting S contents of the slag. The different S contents of **S1** and **S2** are somewhat surprising. From the technical reports of the Barry and Mason Company, it can be deduced that **S1** is older than **S2**, so the difference in S contents of both slag types is taken to reflect either the progressive tuning of the Orkla furnaces operation or the output of the second Orkla furnace when it was being operated for sulphide matte extraction.

Many trace elements are more concentrated in **RS** than in the modern slag, attesting the higher efficiency of the 20th century metallurgy in separating the metal and the slag phases from one another. The great exceptions to this are Zn and Cu, which in the **RS** are 1–2 orders of magnitude less concentrated than in the modern slag. Geological and historical reasoning seems to indicate that the Roman exploitation targeted Cu (and maybe Ag) contained in ores insufficiently known because the relevant archaeological evidence was all but entirely obliterated by the open-pit excavation. Those ores were probably the supergene-enriched zone of the ore-body and the relatively low concentrations of Cu and Zn in the slag attest to the high efficiency of the metallurgical methods used by the Romans, although the lack of Zn should be ascribed not to its intentional extraction but to its vapourisation in a process that passed through a slightly oxidising phase documented by the mineral phases present in **RS**. The **RS** is also high in Pb and Sb. Pb had widespread use in the Roman society, but it is unlikely to have been extracted at S. Domingos, unless the supergene-enriched zone they were mining was particularly lead-rich. In fact, the ancient metallurgy of lead, although simple and widespread, was very inefficient due to lead losses to the slag and to the atmosphere. The high Pb contents of the **RS** (and for that matter, also of the modern one) are due to these difficulties, and its anomalous Sb contents reflect the supergene enrichment of the exploited ore, which was, of course, not available any more when the Orkla furnaces began operation in the first half of the 20th century.

3.4 Slag petrography overview

The prevailing phases in **RS** are glass and silicates (varying from 10 to 56 vol.% and from 33 to 69 vol.%, respectively), the accessory oxides, sulphides, sulphosalts and alloys occupying less than ≈2.5 vol.%; generally, interstitial voids do not rise over 1.5 vol.% and show diameters from the resolution limit to values ranging from ≈24 to 80 μm. The dominant oxide is magnetite, forming skeletal/cruciform grains (Figure 6(**B**)) crystallised out of equilibrium under fast cooling conditions in a groundmass of glass and olivine that, locally, has minor sulphides and sulphosalts (Figure 6(**A**)–(**F**)); when the grain size is relatively large, it can sometimes be seen that S-rich phases clearly postdate magnetite. The main silicate mineral is chemically zoned olivine (Figure 6(**A**) and (**B**)); it forms skeletal 'herring-bone' grains or regular laths several hundred micrometres long, the latter well preserved in the inner parts of the slag fragments where they may coexist either with small and sub-euhedral prismatic grains of melilite or with tiny euhedral pyroxene grains. Pyrite and pyrrhotite are the dominant sulphides and are frequently intergrown with magnetite (Figure 6(**C**)–(**F**)); often, they occur with a complex Pb-rich assemblage, essentially composed of Pb-metal and galena, sometimes with lesser Pb/Sn-sulphoantimonites and Pb-oxides. Occasionally, Cu-rich phases similar to chalcopyrite occur. The glassy domains have fine disseminations of silicates (olivine, eventually also melilite) and of Fe-oxides (magnetite, maybe also wustite), coexisting

with minor Mn-rich phases (mostly pyrolusite); the fractures and voids of these domains are partly sealed by zoned infillings of hematite-goethite.

Figure 6 Petrographic aspects of the slag (**S1** type, unless otherwise stated) (**A**) Backscattered electron image showing euhedral to subeuhedral olivine crystals (medium grey) within pyroxene (dark grey) together with Fe-rich sulphide and oxide phases (light grey); (**B**) Backscattered electron image of the **S2** slag showing cruciform skeletical magnetite crystals (light grey) inside a pyroxene phenocrystal occurring between two olivine laths; (**C**) Reflected polarised day-light image of a typical oxide (dark grey)/sulphide (light grey) intergrowth, together with a clump of exsolving *iss* (central mottled domain); (**D**) Backscattered electron image of **C**, showing lead-bearing phases (small white domains); (**E**) Iron oxide (dark grey)-sulphide (light grey) vermicular intergrowths inside a sulphide bleb. The rounded medium grey domains are the same intergrowth below the resolution limit. The individual intergrowth domains are separated by irregular Cu-rich base-metal sulphide stripes; (**F**) Same as **E**, but with a lesser relative amount of magnetite (dark grey). Here magnetite assumes a plate-like habit representing incomplete skeletal crystals. The lighter zones are mainly Cu-Zn-bearing *iss* crystal (see Table 3 for compositional information)

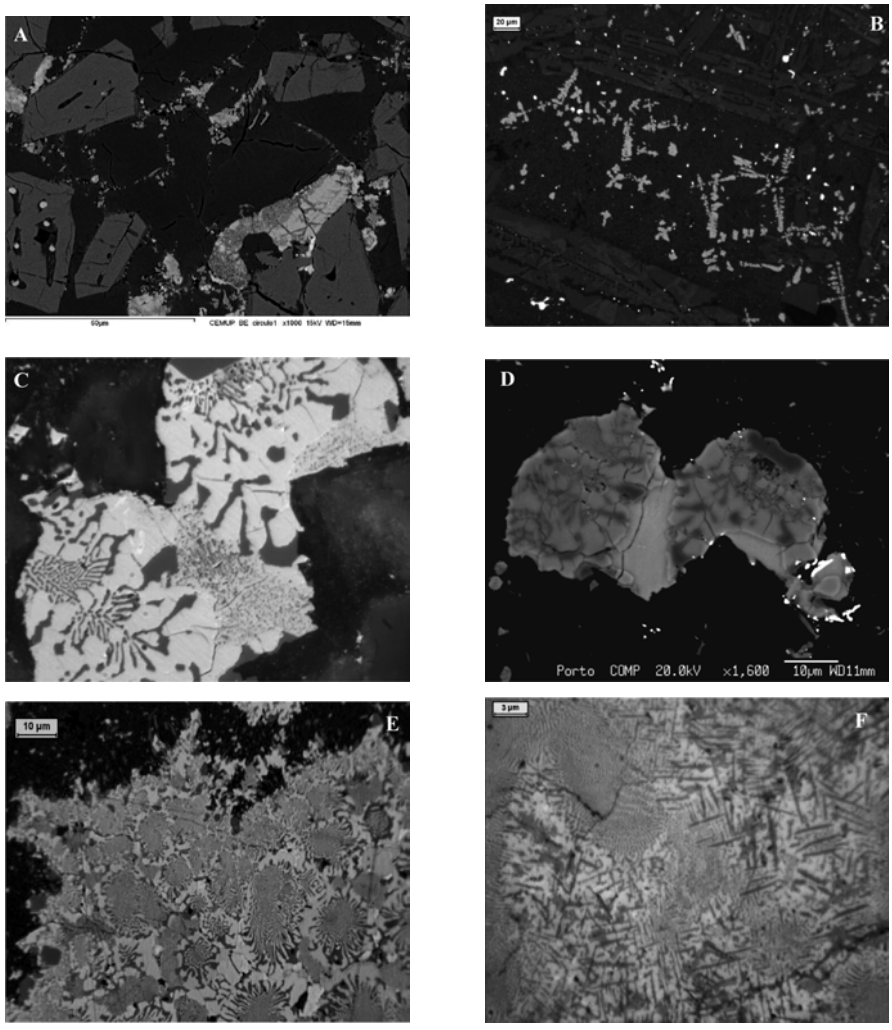

In **S1**, image analysis reveals that, on average, the silicate phases (including glass) occupy nearly 81 vol.%, oxides correspond to ≈2 vol.% and, together, sulphides and alloys to ≈1 vol.%. Porosity is ≈7 vol.%; most of the voids (≈71%) have diameters ranging from 5 to 20 μm. Silicates are mainly olivine and pyroxene, and occur as (sub-)euhedral grains together with tiny (sub-)euhedral magnetite grains in the inner parts of slag fragments. Irregular millimetre oxide/sulphide mixed clusters show wormy intergrowth of spinel in sulphides and, rarely, in silicate glass (Figure 7(**A**)); occasionally, these mixed clusters encircle (sub-)euhedral magnetite grains. The prevailing sulphide is pyrrhotite, often accompanied by pyrite (or eventually marcassite) and very minor amounts of other sulphide phases. Among the latter phases, the Cu-bearing sulphides (mainly chalcopyrite) are the most noteworthy, although Zn-rich phases (akin to sphalerite) can be locally important, sometimes together with rare galena. In these mixed aggregates, a highly reflective intermediate (non-stoichiometric) sulphide phase (*iss*) is also common and shows textures generated by exsolution. **S1** borders are glassy and contain fine to very fine disseminations of oxides (magnetite, maybe also wustite); sporadic silicate micro-crystallites can also be observed, with dendritic textures characteristic of rapid growth. Late hematite (or lepidocrocite?) zoned masses, often botryoidal, seal the most external voids and fractures, and represent the most obvious products of slag weathering.

Fragments of **S2** are composed of roughly 24 vol.% silicates, as elongated olivine and pyroxene prisms with variable aspect ratios, in a dappled silicate glass, sometimes quite heterogeneous; total voids make up, on average, less than 1 vol.%, and have diameters ≤18 μm. In the inner parts of **S2** fragments, prisms are coarse and (sub-)euhedral, often showing strong zoning; at these places, pyroxene crystals are larger than olivine crystals and coexist with euhedral/sub-euhedral magnetite grains. In the outer glassy borders, pyroxene is missing and olivine assumes spinifex textures with very elongated grains, reflecting rapid crystallisation from a significantly undercooled melt. Accessory phases include magnetite (≈4 vol.%) and sulphides; *iss* is rare. In the outer slag domains, the oxide phase (mostly magnetite) develops either micro-cruciform habits or fine dendrites (from several micrometres to tens of micrometres in size) typical of rapid growth under a fast cooling rate. The glassy domains contain, in addition, abundant sulphide-rich droplets with variable size (<2 to 20 μm), trapped within the silicate liquid during the smelting process. Detailed characterisation of the larger droplets reveals different Fe- and Cu-rich phases whose textural relationships show them to result from a pre-existing, swiftly chilled, high-temperature homogeneous phase. The Cu-rich assemblage typical of many droplets is made of chalcopyrite with tawny *iss* exsolutions, occasionally displaying pyrite or pyrrhotite and, rarely, tiny grains of sphalerite, as well as minute *iss* brass-like particles. Galena is rare, but represents a significant accessory phase in some larger droplets (Figure 7(**B**)). The majority of the small sulphide droplets are composed of pyrite (±pyrrhotite), although accessory amounts of chalcopyrite occur, usually in their outer domains. Similar sulphide droplets are randomly distributed in the glassy matrix of the slag inner domains and represent, on average, 0.5 vol.%.

Figure 7 Slag petrographic features. The slag pictured is the Roman slag unless otherwise stated. (**A-1**) Reflected polarised day-light image of Fe-sulphides (pyrrhotite-pyrite-marcassite – light grey) enclosing magnetite crystals (dark grey), sometimes skeletal (**S1** slag); the lighter areas are unresolved complex vermicular intergrowths of Cu- and Pb-bearing sulphides. (**A-2**) Same as (**A-1**), but with less Cu-bearing sulphide; note the skeletal character of magnetite towards the bleb margin; (**B**) – Backscattered electron image of Pb-bearing sulphide (galena – bright white) with vermicular exsolutions of Cu-bearing *iss* sulphides (medium grey) (**S2** slag); (**C**) Reflected polarised day-light image showing metallic Pb (grey) (associated with lesser amounts of Pb-oxides) and Pb-Sb-Sn-sulphosalts (whitish grey); (**D**) Same as C imaged with secondary electrons: metallic Pb (light grey) and Pb-Sb-Sn alloys (dark grey); (**E**) and (**F**) – Details of D at increasing magnifications showing Pb-Sb-Sn alloy grains having up to 18.5 wt% Pb, 59.5 wt% Sb and 34.6 wt% Sn. At large magnification (**F**), it can be seen that at least three different phases coexist (delimited by white dotted lines): metallic Sb (dark grey), $PbSn_6(Sb, As)_9$ (medium grey) and $PbSn_2Sb_6$ (light grey); (**G**) Reflected polarised day-light image showing Sb-Sn-Pb-sulphide (light)-oxide (dark) intergrowths in the ground mass. The bright mineral (arrow) has the highest Sn concentration (up to 4.9 wt% Sn); (**H**) Detail of **G** imaged with backscattered electrons: the phases shown have up to 59.5 wt.% Sb2O5, 19.8 wt.% SnO_2 and 18.7 wt.% PbO; the brighter areas correspond to an Sb-rich phase devoid of Sn and with low Pb concentration

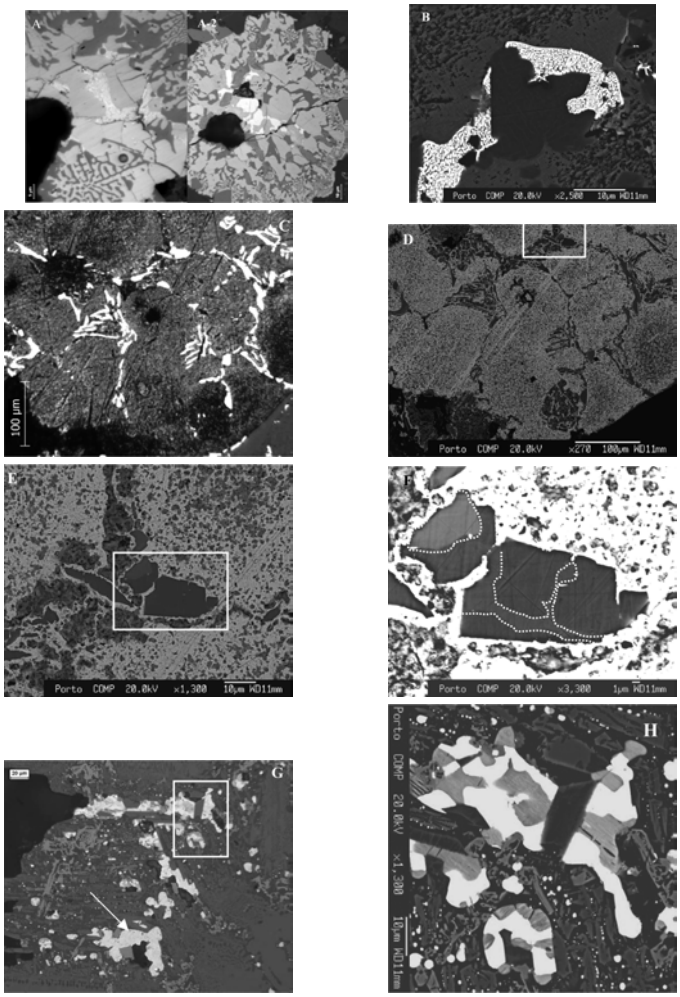

3.5 Slag-forming phases chemistry

Only the most abundant phases visible with the optical microscope (magnetite, olivine, and pyroxene) can be confirmed by XRD; minor phases are not reliably identifiable owing to complex superposition of individual mineral XRD patterns and to signal degradation caused by glass. Point analysis techniques were used selectively to better identify those phases of ambiguous optical features and to gather data on compositional details of sulphide and sulphosalt phases, potentially the major sources both of environmental metal contamination and of recoverable metal contents in case of reprocessing.

3.5.1 SEM-EDS and EPMA data

Olivine grains are Fe-rich (≈68 wt.%), and contain minor amounts of MgO, ZnO, CaO and CuO (up to 0.75, 1.74, 1.16 and 0.40 wt.%, respectively); they are, thus, quasi-pure fayalite displaying limited deviations towards the end-members kirschsteinite ($CaFeSiO_4$) and willemite (Zn_2SiO_4). Large pyroxene grains are close to hedenbergite, but have minor amounts of FeO and ZnO (≈1 wt.% ZnO). The Fe-spinel also shows significant Zn contents (≈1.5 wt.% ZnO); it is magnetite with slight deviations towards the franklinite end-member. Traces of Pb and Cu (≈0.16 wt.% PbO and ≈0.08 wt.% CuO) were also detected in some magnetite grains but these may correspond to sub-microscopic inclusions.

The main sulphide phases (pyrrhotite and lesser amounts of pyrite and marcassite) have Fe-contents ranging from 58.5 to 62.7 wt.% with S varying between 35.7 and 41.3 wt.%. These phases also display traces of Cu (≈0.86 wt.%), Co and Pb (≈0.18 wt.% each), Zn (≈0.17 wt.%) and Cd (≈400 ppm). A few grains of the Fe-sulphides have shown small amounts of gold (up to 600 ppm Au, average 300 ppm Au).

The Cu-bearing sulphides show a relatively wide compositional spectrum, from almost ideal ‘chalcopyrite’ composition to inhomogeneous sulphide masses interpreted as metastable intermediate sulphides (sometimes optically similar to brass), resulting from the partial decomposition of high-temperature Cu-Fe-Zn sulphide solid solutions (Table 3 and Figure 8; Craig, 2001). The first stage in the decomposition is the formation of islands with approximate ZnS composition in “chalcopyrite”, showing textures resembling chalcopyrite disease (Figure 6(**C**)).

Figure 8 Incomplete exsolution of Cu and Zn in *iss*. Cu-bearing sulphides always contain some zinc. The weakness of the correlation is due to variable amounts of Fe

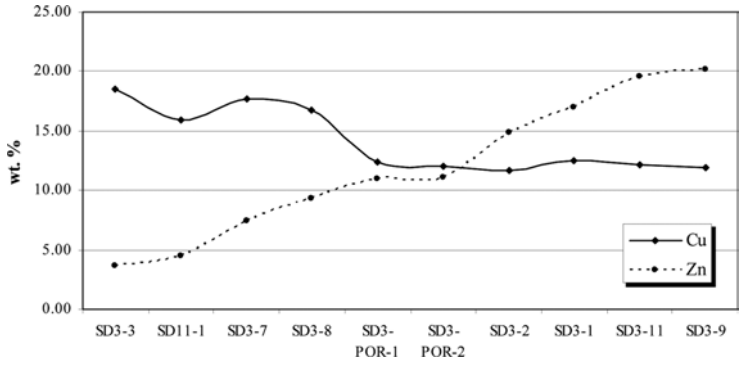

Table 3 Representative EPMA data of Cu-bearing sulphides resulting from partial decomposition of a high-temperature Cu-Fe-Zn sulphide solid solution. Data are expressed in wt %

Element	*SD11-2*	*SD3-3*	*SD11-1*	*SD3-7*	*SD3-8*	*SD3P-1*	*SD3P-2*	*SD3-2*	*SD3-1*	*SD3-11*	*SD3-9*
Fe	19.52	40.35	43.72	38.63	36.99	40.47	40.92	33.74	33.60	31.38	31.88
S	30.65	33.45	34.81	33.98	33.53	33.37	33.19	33.13	33.88	33.20	33.74
Cu	48.30	18.49	15.89	17.66	16.75	12.37	11.97	11.66	12.45	12.14	11.89
Zn	0.13	3.64	4.53	7.47	9.27	10.94	11.11	14.91	17.00	19.60	20.22
Pb	0.26	0.10	0.21	0.10	0.02	0.14	0.19	0.06	0.05	0.09	0.08
Co	0.11	0.09	0.84	0.10	0.11	0.19	0.13	0.13	0.13	0.10	0.09
Cd	0.06	0.06	0.04	0.06	0.05	0.05	0.03	0.01	0.03	0.06	0.04
In	*nd*	*nd*	*nd*	0.03	*nd*	*nd*	0.01	0.05	*nd*	0.04	0.03
Au	0.06	*nd*	*nd*	0.02	0.00	0.01	0.04	0.03	0.04	0.07	0.03
Ge	*nd*	*nd*	*nd*	*nd*	*nd*	*nd*	*nd*	*nd*	0.03	*nd*	*nd*
Ga	*nd*	*nd*	0.03	*nd*	*nd*	*nd*	*nd*	*nd*	*nd*	*nd*	*nd*
Sb	0.04	*nd*	*nd*	*nd*	*nd*	0.02	0.01	0.00	*nd*	0.03	*nd*
Ag	0.14	*nd*	0.01	*nd*	0.01	*nd*	*nd*	*nd*	*nd*	*nd*	*nd*
As	*nd*	*nd*	*nd*	*nd*	*nd*	*nd*	*nd*	*nd*	*nd*	*nd*	*nd*
Mn	*nd*	*nd*	0.04	*nd*	*nd*	*nd*	0.03	*nd*	*nd*	*nd*	*nd*
Tl	*nd*	0.10	*nd*	*nd*	*nd*	0.15	0.08	*nd*	*nd*	0.21	*nd*
Total	99.3	96.6*	100.1	98.1*	96.8*	97.7*	97.7*	94.0*	97.2*	97.0*	98.1*

*Low total reflects micro-porosity in the analysed domain; *nd* = not detected.

Minor and trace elements in Cu-bearing sulphides include Pb (≈0.12 wt.%), Co (≈0.18 wt.%), Cd (≈400 ppm), In (≈300 ppm), Au (≈300 ppm), Sb (≈200 ppm) and Tl (≈1400 ppm); the concentrations of some metals, such as indium, germanium and gallium, are often below detection limit. Compositional maps (Figure 9) show that In, Ge and Ga exist in Cu-bearing sulphide phases; Ge occurs also in Pb-bearing phases. It is possible that In is positively correlated with Zn and Cu, but its low concentration makes this impossible to ascertain; the same is valid for a possible correlation of Ga with Cu and Pb.

Figure 9 Element distribution maps obtained by scanning an electron microprobe over an area of approximately 500 μm^2. A – Iron (Fe); B – Silicon (Si); C – Copper (Cu); D – Indium (In); E – Zinc (Zn); F – Gallium (Ga); G – Lead (Pb) and H – Germanium (Ge). Concentration values are coded by colour; in general, lighter tones represent higher concentrations

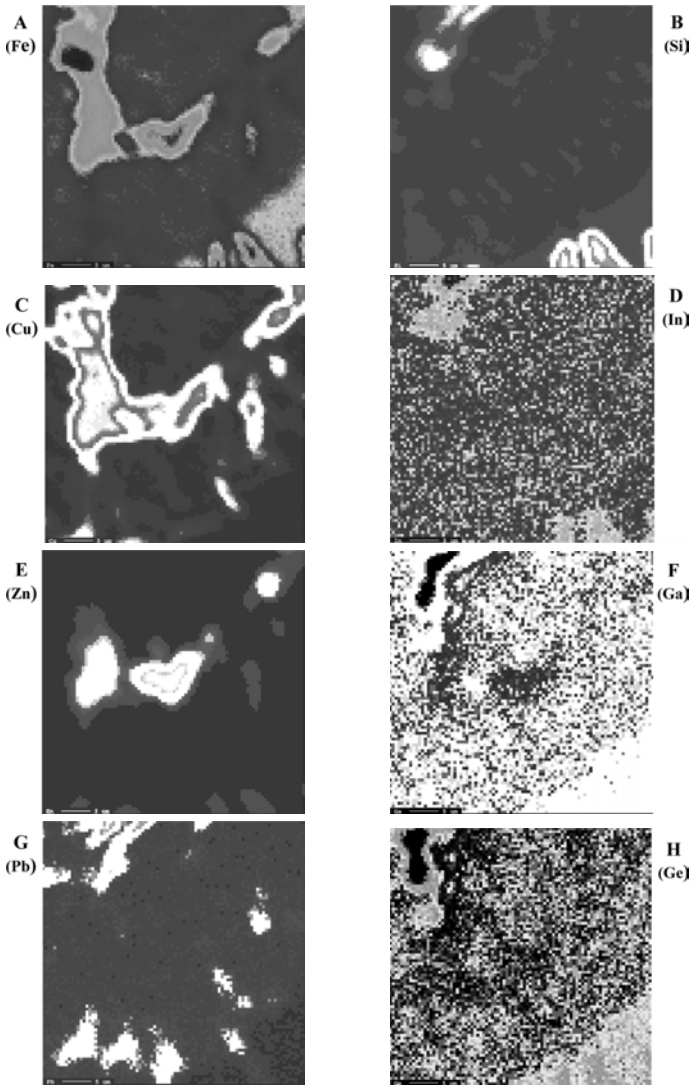

In all the slag types, galena compositionally close to PbS can be observed as very fine vermicular intergrowths both in *iss* and in Cu-Fe-rich sulphides; they are much more common in **RS** than in the modern slag (Figure 6(**E**) and (**F**)). In **S1**/**S2**, owing to small grain size, Pb-rich phases are difficult to characterise: they display 52.6 wt.% Pb but have significant amounts of Fe (up to 16.5 wt.%) and Cu (up to 14.8 wt.%), which may be the result of interference from the surrounding phases (Figure 7(**A-1**) and (**B**)).

In **RS**, Pb occurs as metallic grains (up to 94.3 wt.% Pb), as Pb-Fe-Sn sulphosalts, as Sb-Sn-Pb-oxides and as less abundant galena containing up to 75.4 wt.% Pb with minor amounts of Fe and Sn (up to 2.9 wt.% and 4.6 wt.%, respectively). The composition of Pb-Fe-Sn sulphosalts shows up to 39 wt.% Fe, up to 45 wt.% S and up to 10.8 wt.% Pb, with minor Cu (up to 1.6 wt%) and trace amounts of Sn and Sb (up to 0.4 wt.% and up to 0.3 wt.%, respectively). These phases, especially when carrying Sn and Sb, are often intimately associated with very fine-grained minor amounts of Sb-Sn-Pb-oxides, which, when volumes are big enough to allow proper analysis, were shown to have up to 59 wt.% Sb_2O_5, 20 wt.% SnO and 19 wt.% PbO (Figure 7(**C**)–(**F**)). Occasionally, there are also metallic Sb and Pb-Sn-Sb alloys of variable composition.

The glass phase is Fe-rich and display relatively higher contents of Ca, Zn and Pb in comparison with crystalline silicates. In many surface domains, the glass shows evident compositional zoning, the outer layers being characterised by lower contents of Ca, Zn and Pb. This chemical leaching is often accompanied by the development of an Fe(-Mn)-rich coating, which is compositionally indistinguishable from hematite/lepidocrocite.

3.5.2 μPIXE data

Several representative domains of **RS**, **S1** and **S2** samples were scanned and over the elemental maps obtained 48 spots were selected to perform semi-quantitative point analysis. In general, there is a good correlation between the EPMA and μPIXE data, although the higher sensitivity of the latter method allowed the determination of better values for trace elements in the Fe-dominated sulphides and in magnetite. These sulphides have ≈0.8–9.7 wt.% Cu, ≈0.8–0.9 wt.% Pb, ≈0.5–3.3 wt.% Zn and ≤0.2 wt.% As; the higher Cu and Zn values are probably due to the presence of crypto-inclusions of complex *iss* phases. In magnetite values ≤3.3 wt.% Zn, ≤2.2 wt.% Cu and ≤1.5 wt.% Pb were measured; these values are somewhat higher than those obtained with EPMA but this may be either due to incorrect μPIXE data reduction or an artefact caused by the higher volume probed by μPIXE, therefore integrating a large amount of sulphide or *iss* crypto-inclusions.

Special attention has been paid to the complex Cu-bearing sulphide phases in **S1** and **S2** samples, which display $15.5 \leq Fe \leq 37.7$ wt.%, $0.22 \leq Zn \leq 3.6$ wt.%, $0.35 \leq Pb \leq 0.89$ wt.%, besides traces of Ni (≤0.16 wt.%), Sn (≤0.07 wt.%), Sb (≤0.02 wt.%) and Ag, Cd, In (≤0.01 wt.% each). The presence of crypto-inclusions was again put in evidence by some spots, which contained 3.3–23.8 wt.% Pb. Columns 1–9 in Table 4 show representative semi-quantitative analyses of Cu-bearing phases in a sulphide micro-bleb (Figure 10).

Table 4 µPIXE semi-quantitative results for representative zones of **S1** and **S2** type slag

	S2 slag									*S1 slag*			
Wt%	*1*	*2*	*3*	*4*	*5*	*6*	*7*	*8*	*9*	*1*	*2*	*3*	*4*
Si										15.54		6.28	
S	23.75	26.83	25.84	22.97	27.43	29.16	19.24	25.38	25.57	1.63	30.22	9.68	24.94
Cl										0.22			0.37
K										0.15		0.03	
Ca										3.59	0.15	2.47	0.05
Ti										0.07			
Mn						0.01				0.07	0.03	0.03	0.02
Fe	32.48	24.34	19.68	20.55	30.56	37.15	25.18	24.91	23.82	38.69	40.43	32.37	51.89
Ni	0.05	0.04		0.05	0.14	0.16	0.16	0.04	0.06				
Cu	40.19	47.60	53.91	42.69	36.38	27.42	30.66	46.79	49.44	0.09	17.11	4.99	10.81
Zn	0.19	0.82	0.22	0.29	1.49	2.40	1.00	0.62	0.44	1.22	11.74	0.68	3.22
Pb	3.32	0.37	0.35	13.45	4.00	3.70	23.75	2.25	0.66	0.27	0.32	5.05	8.69
Zr										88	48		
Ag											111	195	208
Cd											62		
In											125		
Sn											472	669	750
Sb												207	178
	99.98	100.00	100.00	100.00	100.00	100.00	99.99	99.99	99.99	61.55	100.08	61.69	100.10

Concentration values in wt% except for Zr, Ag, Cd, In, Sn and Sb which are in µg/g. All elements detected were analysed. Low totals in analyses 1 and 3 in S1 slag are due to non-analysed oxygen. Cl indicates contamination from epoxy used in sample preparation.

Figure 10 Elemental distribution maps of a representative domain containing a sulphide bleb in a **S2** sample. The white spots locate the point analyses of Table 4

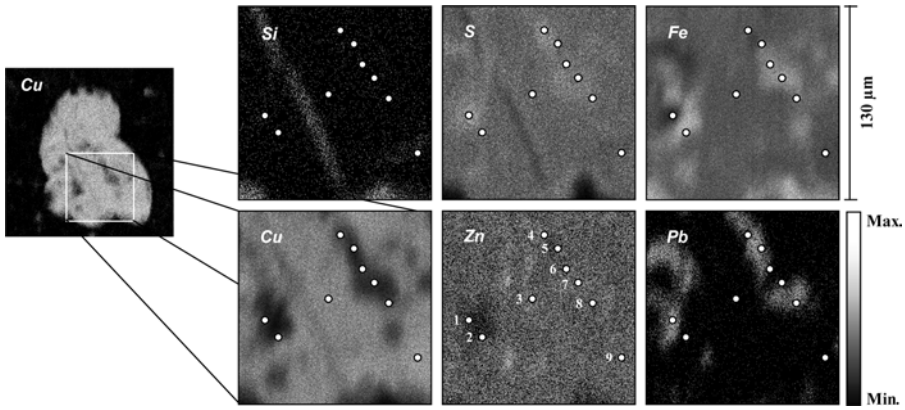

The available µ-PIXE data for the slag glass confirm the presence of Zn (up to 1.22 wt.%) and crypto-inclusions of *iss* phases as revealed by simultaneous high values in S, Pb and Cu (e.g., column 3 of **S1** in Table 4).

4 Discussion

Slag characteristics mainly reflect the chemical composition of the ores and additives used in smelting, and are also strongly influenced by the temperature and cooling rates of the melts, which originate them. During the smelting process, the density and viscosity of the molten slag have to be kept low enough to ensure the gravity separation of the metal-rich liquids (sulphide matte). Under ideal conditions, silicate slag should float on the surface of the sulphide matte, concentrating the oxide components of the silicate gangue and additives. Nonetheless, metal-rich droplets unable to decant in time will be incorporated in the slag, as observed.

The relative abundance of Fe-olivine (theoretically formed at 1100–1177ºC) strongly suggests that the furnace temperature was at least 1200ºC. The melts produced are not very rich in Ca; the available Ca is incorporated in the early-formed pyroxene and the subsequent olivine, coeval with magnetite, is already Ca-poor. The dominance of these crystalline silicates, together with the absence of melilite in **S1/S2**, indicate that the slag was cooled and quenched quickly or at least under a fairly fast cooling rate; this is consistent with the observed textures. When the cooling rate is too fast, pyroxene crystallisation is inhibited, olivine crystallises with spinifex texture and magnetite develops a dendritic habit.

As crystallisation of the silicate melt proceeds, the available base-metal content will be redistributed among several silicate crystalline phases, residual glass and sulphide matte. In **S1/S2**, most of the Cu enters the sulphide matte upon consolidation of the silicate melt. Zinc is volatile and soluble in the silicate melt (Ettler et al., 2001 and references therein) and is known to condense or separate as ZnO and ZnS phases trapped in the molten slag (Chaudhuri and Newesely, 1993) or to enter early mineral structures. In the S. Domingos case, these processes seem to have led to limited Zn fixation, as both olivine and spinel are very low in this metal and the amount of independent Zn-bearing

sulphides is also relatively low. Therefore, as most of the zinc occurs dissolved in the glass, it seems logical to conclude that most of the original Zn has been lost to the atmosphere through vapourisation. Lead has a similar distribution in the slag, but this is due to its incompatible behaviour, i.e., due to its inability to enter the normal silicate-oxide mineral structures. Under equilibrium, Pb would form its own mineral phases (normally galena, if S is available); its presence in the glass may attest either fast non-equilibrium incorporation in the glass structure or, as suggested by some μ-PIXE analyses, the formation of sulphide crypto-inclusions. Interestingly, galena and other Pb(Sb, Sn)-bearing minerals are indeed found in **RS**; this is not, however, evidence for lower cooling rate and must reflect different ore composition (the Romans were exploiting the iron-hat, not the primary sulphide ore) or differences in the pyrometallurgical processes used. The identification of PbO and Pb^0 indicates that the chemical conditions in the Roman furnace may have been slightly oxidant and, incidentally, that the industrial process was unable to recover efficiently the produced lead.

Slag is typically porous and chemically reactive, forming secondary mineral phases by reaction with air and surface waters. The surface-deposition zone probably results from the dissolution of the nearby metallic fraction (massive matte or sulphide–metallic inclusions trapped within the glass), followed by precipitation of secondary phases from the metal-rich solutions. The chemical composition of these precipitates, as well as of those filling late fractures, is variable, although clearly dominated by a complex mixture of Fe oxy-hydroxides locally enriched in Cu-, Fe- (and Pb-) sulphates. The potential environmental hazard posed by the slag increases with its glass contents (Eusden et al., 1999; quoted by Ettler et al., 2001). The hazard quantification is at present impossible in both slag types but the intensity of the weathering effects is not very high, as shown by the slight development of the alteration rims, provided the slag accumulations are left undisturbed.

It should be noted that both types of the São Domingos slag (like many other Fe-rich and air-cooled slag) show favourable mechanical properties for aggregate use, including excellent sound characteristics, good abrasion resistance and good stability (high friction angle owing to the sharp fragment shapes). However, the slag reuse will imply its continuous mechanical disturbance and this will cause the release of considerable amounts of metals due to erosion of the slag and its weathering products. Therefore, the slag should not be put to use without a previous programme of re-smelting or other alternative chemical handling to reduce its metal release ability. During this treatment, economic recovery of metals cannot be ruled out, since the envisaged programme will result in better silicate crystallisation, separate precipitation of the incompatible metals and eventual separate recovery of all elements (including S) now forming the sulphide/sulphosalt phases.

5 Conclusions

The long mining history of S. Domingos led to the production of large volumes of residues, including several metal-rich slag piles that account for about 8% of the discarded waste. These slag piles represent two different epochs of mining, the initial Roman exploitation and the final modern activity (1934–1962); up to the present, no slag of intermediate age has been recognised.

Both slag types are mainly composed of silicate glass and crystalline silicates (fayalitic olivine and hedenbergitic pyroxene) with minor amounts of magnetite and Fe(-Zn) sulphides. They also contain lesser Cu-Zn-bearing non-stoichiometric sulphide phases and traces of sulphosalts; **RS** is further characterised by the presence of melilite and of Pb, Sb and Sn phases (sulphides, sulphosalts, alloys, oxides and Pb and Sb metals). Mineral and textural features observed denote variable but fast cooling rates, normally faster at the borders and slower inside the slag fragments; a similar rim to core gradient of cooling rates can also be inferred from the textures preserved at sulphide blebs immersed in silicate masses. Significant amounts of metal remain in both slag types, dissolved in glass, incorporated in the silicate mineral structures and also in the sulphide blebs, where they may form minerals of their own (sometimes including alloys and free metals).

The main differences between the two slag types are due to differences in ore composition and in processing technologies. It is notable that such different ore-processing technologies as used by the Romans and in the first half of the 20th century have resulted in similar slag compositions, although displaying significant textural differences due to different cooling rates.

The available data shows that slag is chemically reactive under weathering conditions. As expected, the most unstable phases are those occurring in the sulphide blebs and silicate glass; the latter tends to lose its metal content and the former dissolve and partially re-precipitate as Fe(-Mn) (hydr-)oxides and base metal sulphates. Despite their great age difference, the **RS** is not much more weathered than the modern one. The main difference is the presence in the **RS** of a continuous Fe(-Mn)-hydroxide coating that partially isolates the slag fragments from the weathering agents, in what amounts to natural attenuation of their environmental impact. This coating is under development on the modern slag, but any mechanical disturbance of the slag piles will interrupt the process and restore the initial chemical reactivity of the slag. The slag has potential to be reused as an aggregate material, provided this chemical reactivity is significantly reduced by means of reprocessing, which may lead to metal recovery from the slag.

Slag piles are a common feature at the old mining centres of the IPB, both in Portugal and in Spain. In both countries, slag is often being used for road pavements, owing to its excellent physical properties. However, this usage may be premature and inconsidered, since the slag may potentially contain recoverable and valuable metal contents. Moreover, its use without any prior chemical inertisation is sure to lead to potentially serious environmental contamination, because the abrasion caused by vehicle wheels will continuously expose new material to weathering in a setting where the weathering products will inescapably interact with the human population.

Acknowledgements

This work was funded by FCT through project METALTRAVEL (POCTI/ CTE-GEX/61700/04). The manuscript revisions made by two anonymous referees are thanked.

References

Ally, M.R., Berry, J.B., Dole, L.R., Ferrada, J.J. and Van Dyke, J.W. (2001) 'Economical recovery of by-products in the mining industry', *Oak Ridge National Laboratory*, ORNL/TM-2001/225, p.26.

Alves, L.C., Breese, M.B.H., Alves, E., Paul, A., Da Silva, M.R., Da Silva, M.F. and Soares, J.C. (2000) 'Mícron-scale analysis of SiC/SiCf composites using the new Lisbon Nuclear Microprobe', *Nucl. Instrum. Meth.*, Vol. B161–B163, pp.334–338.

Atzeni, C., Massidda, L. and Sanna, U. (1996) 'Use of granulated slag from lead and zinc processing in concrete technology', *Cement Concrete Res.*, Vol. 26, p.1381.

Barriga, F.J.A.S., Carvalho, D. and Ribeiro, A. (1997) 'Introduction to the Iberian pyrite belt', in Barriga, F.J.A.S. and Carvalho, D. (Eds.): *Geology and VMS Deposits of the Iberian Pyrite Belt, SEG Neves Corvo Field Conference 1997*, Guidebook Series, Vol. 27, pp.1–20.

Batista, M.J. (2000) 'Environmental state of the Portuguese test site S. Domingos mine: past and present', *Report European Commission*, http://www.brgm.fr/mineo/IGM_test_site.pdf, p.41.

Bayliss, P., Erd, R.C., Mrose, M., Roberts, A.C. and Sabina, A.P. (1993) 'Mineral powder diffraction file databook', *International Center for Diffraction Data*, Park Lane, Pennsylvania.

Bryan, C., Hallberg, K.B. and Johnson B.D. (2006) 'Mobilisation of metals in mineral tailings at the abandoned São Domingos copper mine (Portugal) by indigenous acidophilic bacteria', *Hydrometallurgy*, Vol. 83, pp.184–194.

Carvalho, D. (1971) 'Mina de São Domingos', *Jazigos Minerais do Sul de Portugal*, Livro Guia nº 4, pp.59–64.

Carvalho, D., Barriga, F.J.A.S. and Munhá, J. (1999) 'Bimodal-siliciclastic systems – the case of the Iberian Pyrite Belt', *Reviews in Economic Geology*, Vol. 8, pp.375–408.

Chaudhuri, J.N.B. and Newesely, H. (1993) 'Mineralogical characterization of old Harz Mountain slags', *Can. Metall. Quart.*, Vol. 32, pp.1–12.

Craig, J.R. (2001) 'Ore-mineral textures and the tales they tell', *Canadian Mineral.*, Vol. 39, pp.937–956.

Custódio, D. (1996) 'Sistemas de lavra na Mina de São Domingos', *Mineração Baixo Alentejo*, C.M. Castro Verde, Vol. I, pp.174–185.

Ettler, V.E., Legendre, O., Bodénan, F. and Touray, J-C. (2001) 'Primary phases and natural weathering of old lead-zinc pyrometallurgical slag from Príbram, Czech Republic', *Canadian Mineral.*, Vol. 39, pp.873–888.

Eusden, D.J., Eighmy, T.T., Hockert, K., Holland, E. and Marsella, K. (1999) 'Petrogenesis of municipal solid waste combustion bottom ash', *Appl. Geochem.*, Vol. 14, pp.1073–1091.

Evanko, C.R. and Dzombak, D.A. (1997) 'Remediation of metals-contaminated soils and groundwater', *Carnegie Mellon University*, TE-97-01, p.53.

Gaspar, O.C. (1998) 'História da mineração dos depósitos de sulfuretos maciços vulcanogénicos da Faixa Piritosa Portuguesa', *Boletim de Minas*, Vol. 35, No. 4, pp.401–414.

Gee, C., Ramsey, M.H., Maskall, J. and Thornton, I. (1997) 'Mineralogy and weathering processes in historical smelting slag and their effect on the mobilisation of lead', *J. Geochem. Explor.*, Vol. 58, pp.249–257.

Grime, G.W. and Dawson, M. (1995) 'Recent developments in data acquisition and processing on the Oxford scanning proton microprobe', *Nucl. Intrum. Meth.*, Vol. B104, pp.107–113.

Kucha, H., Martens, A., Ottenburgs, R., De Vos, W. and Viaene, W. (1996) 'Primary minerals of Zn–Pb mining and metallurgical dumps and their environmental behaviour at Plombières, Belgium', *Environ. Geol.*, Vol. 27, pp.1–15.

Mason & Barry Company (1962) 'Cartografia mineira do jazigo de São Domingos', *Archives of INETI*, Lisboa, Portugal.

Matos, J.X. (2004) 'Carta geológico-mineira de São Domingos, esc. 1/5000', *Instituto Geológico e Mineiro*, Lisboa, Portugal.

Matos, J.X. and Martins, L. (2006) 'Reabilitação ambiental de áreas mineiras do sector português da Faixa Piritosa Ibérica: estado da arte e perspectivas futuras', *Bol. Geológico y Minero España*, Vol. 117, pp.289–304.

Matos, J.X., Pereira, Z., Oliveira, V. and Oliveira, J. (2006a) 'The geological setting of the São Domingos pyrite orebody, Iberian Pyrite Belt', *Proceedings of VII Cong. Nac. Geol.*, Estremoz, Portugal, pp.283–286.

Matos, J.X., Soares, S. and Claudino, C. (2006b) 'Caracterização geológica-geotécnica da corta da mina de S. Domingos, FPI', *Proceedings of X Cong. Nac. Geotécnica, Soc. Port. Geotecnia*, Univ. Nova de Lisboa, Portugal, Vol. 3, pp.741–752.

Matos, J.X., Peterson, E.U. and Chávez, W.X. (2003) *Environmental Geochemistry Field Course, Iberian Pyrite Belt*, SEG Guidebook, Beja, Portugal, p.32.

Maxwell, J.A., Teesdale, W.J. and Campbell, J.L. (1995) 'The guelph PIXE software package II', *Nucl. Instrum. Meth.*, Vol. B95, pp.407–421.

Moore, J.N. and Luoma, S.N. (1990) 'Hazardous wastes from large-scale metal extraction', *Environ. Sci. Technol.*, Vol. 24, No. 9, pp.1279–1285.

Nagasua, H. (1979) 'Basic research for chlorination of copper and zinc in copper converter slag', *Trans. Inst. Met.*, Vol. 20, No. 9, pp.483–492.

Oliveira, J.T. and Matos, J.X. (2004) 'O caminho de ferro da mina de S. Domingos ao Pomarão: um percurso geo-educacional na Faixa Piritosa Ibérica', *XXIV Encontro Prof. Geociências APG*, p.19.

Oliveira, J.T. and Silva, J.B. (1990) 'Carta Geológica de Mértola Fl. 46D na escala 1/50000', *Serviços Geológicos de Portugal*, Lisboa, Portugal.

Oliveira, J.T., Relvas, J.M.R.S., Pereira, Z., Matos, J.X., Rosa, C.J., Rosa, D., Munhá, J.M., Jorge, R.C.G.S. and Pinto, A.M.M. (2006) 'O Complexo Vulcano-Sedimentar da Faixa Piritosa: estratigrafia, vulcanismo, mineralizações associadas e evolução tectonoestratigráfica no contexto da Zona Sul Portugesa', *Geologia de Portugal no contexto da Ibéria*, VII Cong. Nac. Geologia, Univ. Évora, Portugal, pp.207–244.

Silva, J.B., Oliveira, O., Matos, J.X. and Leitão, J.C. (1997) 'Aljustrel and the Central Iberian Pyrite Belt', in Barriga, F.J.A.S. and Carvalho, D. (Eds.): *Geology and VMS Deposits of the Iberian Pyrite Belt*, SEG Neves Corvo Field Conference 1997, Guidebook Series, Vol. 27, pp.73–124.

Tümen, F. and Bailey, N.T. (1990) 'Recovery of metal values from copper smelter slags by roasting with pyrite', *Hydrometallurgy*, Vol. 25, pp.317–328.

Vara, I.P. (1963) *Piritas de Huelva, su historia, míneria y aprovechamiento*, Summa, Madrid, p.1003.

Webb, J. (1958) 'Observations on the geology and origin of the San Domingos pyrite deposit. Portugal', *Comun. Serv. Geol. Portugal*, Vol. 42, pp.119–143.

Ziyadanoğullari, B. and Ziyadanoğullari, R. (1999) 'The recovery of copper and cobalt from oxidized copper ore and converter slag', *Turk. J. Chem.*, Vo. 23, pp.51–55.